JACS
JOURNAL OF THE AMERICAN CHEMICAL SOCIETY
Article
pubs.acs.org/JACS

C−Au Covalently Bonded Molecular Junctions Using Nonprotected Alkynyl Anchoring Groups

Ignacio José Olavarria-Contreras,[†] Mickael L. Perrin,[†] Zhi Chen,[‡] Svetlana Klyatskaya,[‡] Mario Ruben,[‡,¶] and Herre S. J. van der Zant*,[†]

[†]Kavli Institute of Nanoscience, Delft University of Technology, Lorentzweg 1, Delft 2628 CJ, The Netherlands
[‡]Institute of Nanotechnology (INT), Karlsruhe Institute of Technology (KIT), 76344 Eggenstein-Leopoldshafen, Germany
[¶]IPCMS-CNRS, Université de Strasbourg, 23 rue de Loess, 67034 Strasbourg, France

Supporting Information

ABSTRACT: We report on an approach to realize carbon−gold (C−Au) bonded molecular junctions without the need for an additive to deprotect the alkynyl carbon as endstanding anchor group. Using the mechanically controlled break junction (MCBJ) technique, we determine the most probable conductance value of a family of alkynyl terminated oligophenylenes (OPA(n)) connected to gold electrodes through such an akynyl moiety in ambient conditions. The molecules bind to the gold leads through an sp-hybridized carbon atom at each side. Comparing our results with other families of molecules that present organometallic C−Au bonds, we conclude that the conductance of molecules contacted via an sp-hybridized carbon atom is lower than the ones using sp^3 hybridization due to strong differences in the coupling of the conducting orbitals with the gold leads.

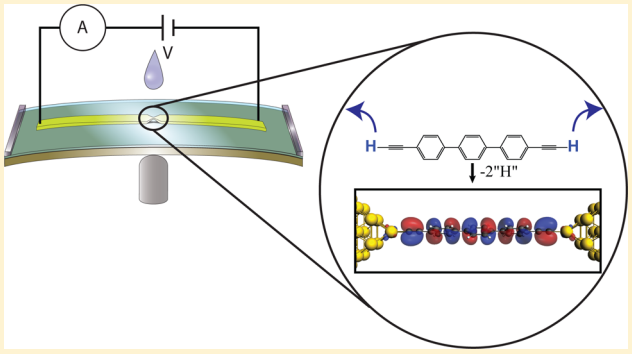

INTRODUCTION

Recent developments in break-junction measuring techniques[1−4] have allowed researchers to investigate charge transport through individual molecules. Strategies for contacting molecules to metallic electrodes usually rely on the use of anchoring groups such as thiols,[5] cyano,[6] pyridines,[7] or amines[8−10] and systematic comparisons have been carried out.[11−14] Recently, new methods have been developed to contact molecules based on a direct carbon−gold bond.[15−22] These methods employ protection groups at the extremities of the molecule that, by applying different external stimuli, are removed in the solvent leaving the endstanding carbon atoms free to coordinate directly to the gold atoms of the electrodes. It has been shown that direct a carbon−gold bond can give rise to a high molecular conductance.[17]

Molecules composed of a series of phenyl rings, such as oligphenylenes (OP), oligophenylethylenes (OPE), or oligophenylvinylenes (OPV), are interesting systems because they possess delocalized orbitals allowing for efficient charge transport. Several research groups have reported on transport through single-molecule junctions with a direct C−Au bond using these conjugated molecular backbones.[16−21] W. Chen et al.[17] have studied a family of highly conductive OPn (n = 1−4) molecules, which form a covalent C−Au bond by cleaving $SnMe_3$ protecting groups, exposing a methylene (sp^3-hybridized carbon). The same research group also reported on the conductance of a *para*-phenyl (OP1) molecule connected by an sp^2-hybridized carbon to the gold using the same $SnMe_3$ leaving groups.[16] Hong et al.[18] performed measurements on a trimethylsilyl oligophenylethylene (TMS-OPEn, n = 1, 2, or 3) family of molecules. Using tetrabutylammonium fluoride (TBAF) as a deprotecting agent, they cleaved the TMS end group from the oligophenylethylene backbone leaving an sp-hybridized carbon free to form a Au−C σ-bond. Despite the advantages of the C−Au bonding, there are also drawbacks to the reported approaches, including the rapid formation of dimers, the need for a deprotecting agent, or rather toxic precursors as leaving groups.

Here, we report on the measurement of the low-bias conductance on a family of oligo(phenyl ethynylene), OPAn, molecules, displayed in Figure 1a, in which the alkynyl end-group (R−C≡C−H) acts as an anchoring group. These molecules directly form a C−Au bond to the leads by the in situ deprotonation of the acidic C−H proton ($pK_a \approx 26$) of the alkynyl groups.[23−25] This approach avoids the need for deprotecting agents or toxic leaving groups. Moreover, the molecules do not exhibit bulky protective groups. Measurements are performed using the mechanically controlled break junction (MCBJ) technique in ambient conditions and show the formation of molecular junctions even after several hours after deposition; the conductance values are of the same order

Received: April 1, 2016
Published: June 7, 2016

ACS Publications © 2016 American Chemical Society

DOI: 10.1021/jacs.6b03383
J. Am. Chem. Soc. 2016, 138, 8465−8469

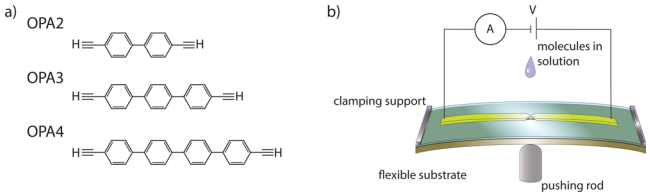

Figure 1. (a) Chemical structure of the molecules studied in this work. Phenylene hydrogen atoms are omitted. (b) Schematics of the mechanically controlled break junction (MCBJ) set up.

of magnitude as similar molecules with sp- or sp^2-hybridized Au−C bonds while being an order of magnitude lower than those using sp^3 Au−C hybridization.[16]

■ RESULTS AND DISCUSSION

Figure 2 displays the conductance vs electrode displacement histograms of three oligo(phenyl ethynylene) molecules: (a) OPA2, (b) OPA3, and (c) OPA4. In each of these diagrams, we identify two characteristics. First, an exponential conductance decay is present between 0 and 0.5 nm covering the conductance range from about $10^{-4}G_0$ to the noise level (marked with thin black lines); these breaking traces are attributed to empty junctions. The color scale indicates that in most of the cases no molecule has been trapped between the electrodes. The second characteristic is a region where the conductance decreases more slowly with stretching. Examples of individual traces in this regime are displayed in the insets of Figure 2. OPA3 (Figure 2b) exhibits this region between displacements ranging from 0 to 1 nm with a conductance around $10^{-3}G_0$. For OPA4 (Figure 2c), the same behavior is observed between 0 and 1.5 nm with a conductance around $10^{-4}G_0$. OPA2 needs a closer look, because it presents two such regions; the first one, around $10^{-3}G_0$, is characterized by displacements shorter than 0.6 nm and a second high-count region is present near $10^{-5}G_0$ for traces between 0.5 and 2.5 nm. An interesting feature is that most of the traces show slanted plateaus rather than flat ones as is usually seen in molecular wires.

We have also performed the same experiment on a phenyl ethylene (OPA1) molecule, but we did not observe clear molecular signatures in that case; see the molecular structure and histograms in Figure S3 in the SI. In ref 18, a similar single phenyl ring with an unprotected alkynyl anchoring group was measured: Junction formation was not observed there either while the same backbone with a TMS protecting group showed molecular features.

To determine the conductance value of the OPA*n* molecules, we constructed one-dimensional conductance histograms without any data selection (Figure 3a). By fitting a log-normal

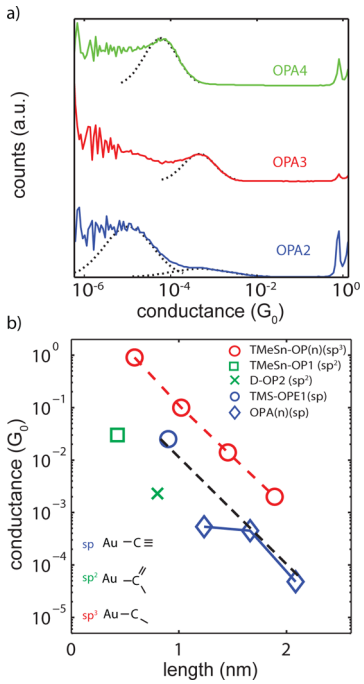

Figure 3. (a) One-dimensional conductance histograms using a logarithmic binning (solid line) for OPA2 (blue), OPA3 (red), and OPA4 (green). Dotted lines represent log-normal fittings around the regions of high counts in the histograms and are used to extract the most probable conductance value. (b) Conductance as a function of molecular length for OPA*n* (blue) compared with other molecules in the literature that form direct C−Au bonds. Different families present different hybridization of the last carbon. Red open circles represent molecules with direct sp^3 C−Au bonding from ref 17; the green square is a single benzene ring connected to gold through an sp^2-hybridized carbon;[16] the open blue circle corresponds to OPE1 connected to gold via an sp-hybridized carbon from the series in ref 18; the green × is a diazonium terminated OP2, which is electrochemically deprotected and connected through an sp^2-hybridized carbon that was studied in ref 20. The black dashed line connects the OPA*n* series. Note that the structure of OPE1 corresponds to the same structure as OPA1 in this study when contacted to the gold electrodes.

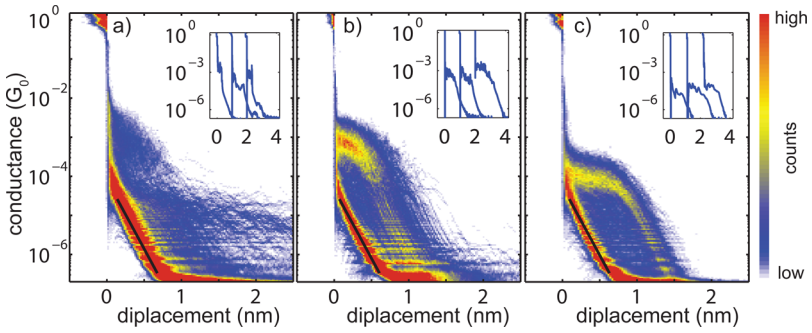

Figure 2. Two-dimensional conductance vs electrode displacement histograms constructed from 2000 consecutive breaking traces measured at room temperature in air with a 0.1 V bias voltage applied and a ramp rate of 10 nm/s. Junctions exposed to a 28 μM molecule solution in dichloromethane for (a) OPA2, (b) OPA3, and (c) OPA4. Insets show examples of individual conductance traces with plateau-like features assigned to the presence of a molecule; traces are offset in the displacement direction.

DOI: 10.1021/jacs.6b03383
J. Am. Chem. Soc. 2016, 138, 8465−8469

distribution to the conductance regions with molecular features (dotted lines in Figure 3a), we extracted the most probable molecular conductance value for the three molecules; for each molecule, two samples were measured. The values of the obtained conductance are summarized in Table 1, and the average values are plotted with blue diamonds as a function of molecular length in Figure 3b. For OPA2, two values of conductance are listed, one at high conductance and one at low conductance, corresponding to the two features appearing in the two-dimensional histogram. We attribute the highest one to the molecular conductance of the molecule itself, whereas the lower value with plateau lengths exceeding the length of the molecule can be associated with the presence of dimers of the molecule[18,19] or to $\pi - \pi$ stacking of two molecules each attached to one electrode.[26] For this molecule, we have analyzed the time evolution of the conductance vs displacement curves in time to investigate whether the dimer formation occurs more frequently as times progresses. We have not found a clear indication for such a trend (see Figure S4): after 4 h of measurements, high and low-conductance traces are still present.

Table 1. Most Probable Molecular Conductance for the Series of OPA*n* molecules extracted from the one-dimensional conductance histograms[a]

molecule	conductance (G_0)	
OPA2	6.6×10^{-4}, 1.0×10^{-5}	4.1×10^{-4}, 7.8×10^{-6}
OPA3	4.6×10^{-4}	4.4×10^{-4}
OPA4	5.7×10^{-5}	3.9×10^{-5}

[a]The first column contains the values obtained with a concentration of 28 μM, and the values in the second column were obtained with a saturated concentration of molecules, meaning 4.95 mM for OPA2, 0.36 mM for OPA3, and 28 μM for OPA4. The values plotted in Figure 3 are the average of the two measurements of each molecule. For OPA2, two values are listed, one at high conductance and one at low conductance (see text for a discussion on these values).

A striking characteristic of Figure 3b is the nonexponential decay of the conductance with molecular length (open blue diamonds) for the OPA*n* (n = 2, 3, 4) series. The fact that the conductance of OPA2 has approximately the same value as OPA3 is an unexpected result, especially because measurements on the same molecular backbone (oligophenylene) have shown an exponential decay for different anchoring groups and measurement techniques,[17,27−29] with $\beta \approx 0.45$ Å^{-1}. An interesting observation is that the deprotonated OPA1 has the same structure as the deprotected TMS-OPE1 in ref 18. If we take into account this conductance value, an exponential decay among OPE1, OPA3, and OPA4 (black dashed line in Figure 3b) is found.

To put our results in a broader context, we compare our data with other molecules that also form direct Au−C bonds to the leads. The conductance vs length dependence of these molecular families is displayed in Figure 3b as well. We observe that the conductance of molecular chains that are connected via sp^3-hybridized carbon atoms is higher than the corresponding chain connected by sp-hybridized carbon atoms. For the single benzene ring case, this observation was already discussed in ref 17 when comparing sp^3- and sp^2 hybridization.

We have also performed density functional theory (DFT) calculations to compute the molecular geometries and electronic structure of OP*n* (n = 2, 3, 4) chains with sp- and sp^3 hybridization of the anchoring carbon atoms, corresponding to OPA*n* and SnMe−OP*n* structure inside the junction, respectively. These calculations were combined with the nonequilibrium Green's function (NEGF) formalism to obtain the transmissions; self-energies were corrected using the DFT + Σ method.[8] Figure 4a,b shows the iso-surface of the highest occupied molecular orbital (HOMO) for OP3 with an sp- and sp^3-hybridized anchoring carbon, respectively. The lower panels display the same orbitals in the region where the molecule contacts the gold. We note two important differences. First, the amplitude of the wave functions around the linking gold is smaller in the case of sp, and second, the symmetry of the atomic orbital of the gold atom that is involved in the wave function is different in the two cases. In the case of sp hybridization, the main contribution of the gold to the wave function comes from the 5d orbital, while in the case of the sp^3-hybridized carbon, the main contribution comes from the 6s orbital of the gold.

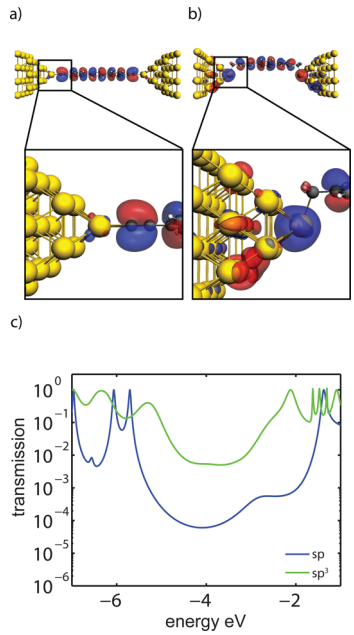

Figure 4. Diagram of the HOMO of a OP3 attached to gold atoms through (a) sp- and (b) sp^3-hybridized carbon. Zoom ins (lower panels) show the same orbitals near the Au−C interface. (c) Transmissions calculated using DFT+NEGF for the OP3 molecule with sp- (blue line) and sp^3-hybridized (green line) linking to the gold.

Focusing on the transmission function of OP3 as displayed in Figure 4c, one notes that in the case of sp^3 (green drawn line) the shape of the resonance peaks is broader, indicating a higher coupling between the electrodes and the molecule, in agreement with the wave function overlap discussion earlier. The calculations further support our findings that the conductance of molecules with the same number of benzene rings differs greatly depending on the hybridization of the end-standing carbon atoms: sp^3-hybridization gives a higher conductance, mainly because the favorable coupling between the gold electrodes and the molecule.

We also analyzed the dependence of the conductance on the molecule length and found that the transmission function decays exponentially with molecular length for the sp-hybridized OPA*n* series as can be seen in Figure S7. The odd behavior of the OPA2 conductance, therefore, may be

DOI: 10.1021/jacs.6b03383
J. Am. Chem. Soc. 2016, 138, 8465−8469

associated with degrees of freedom not captured in the calculation. For example, a nonexponential decay of conductance has also been observed for oligothiophene molecules,[30,31] and in that case, it was attributed to the ability of a 4-thiophene to rotate toward a more conjugated configuration compared with the 3-thiophene, which cannot rotate. Another explanation may originate from the binding configuration itself. In the literature, it has been proposed that alkynyl groups in contact with gold may form a rather "undetermined" binding configuration displaying a more sp^2 like character;[23,32−34] the smaller the molecule, the more this is expected to occur.[35] This suggestion is in line with the results displayed in Figure 3, which show that a line parallel to the black and red drawn lines through the sp^2-hybridized OP1 and diazonium terminated OP2 data points (open square and the green ×, respectively) interestingly is close to the OPA2 conductance value from our study.

In conclusion, we have demonstrated that it is possible to contact single molecules through a covalent σ-C−Au bond formation directly from deprotonating alkynyl anchoring groups. This method avoids the need for cleavage of bulky protecting groups and the use of deprotection by an external agent. In our approach, the molecules connect to the gold leads through an sp-hybridized carbon atom in a way that it mainly couples to the 5d orbital of the gold. The involvement of the 5d orbital leads to a lower electronic coupling than for sp^3-hybridized carbon, which involves the 6s orbital of gold.

METHODS

Synthesis. The molecules OPA2 and OPA3 were synthesized following reported procedures.[36,37] For the synthesis of OPA4, a novel procedure was developed. The detailed description and characterization of OPA4 can be found in the SI.

Conductance Measurements. Single-molecule conductance measurements were performed in a mechanically controllable break junction (MCBJ) set up.[38] The devices consist of a phosphorus bronze flexible substrate coated with a polyimide insulation layer, on top of which a lithographically defined gold wire with a constriction is patterned. The narrower part of the wire is suspended by reactive ion etching of the polyimide. The substrate is then clamped at both ends and bent by the action of a pushing rod beneath the center of the substrate (Figure 2b) until the gold wire breaks leaving two atomically sharp electrodes separated by a nanoscale gap. The electrodes are fused and broken thousands of times at a rate of 10 nm/s. During this process, the conductance ($G = I/V$) is recorded using a logarithmic amplifier with a bias voltage of 0.1 V. During each breaking process, the conductance is recorded as a function of the electrode displacement. Before the gold wire breaks, the conductance of the junction drops in a stepwise manner due to atomic rearrangements in the contact. When the metallic contact breaks, the conductance sharply drops below 1 G_0, where G_0 is the conductance quantum ($G_0 = 2e^2/h$ with h being the Planck's constant and e the charge of an electron). This sharp decrease in conductance is used to set the zero displacement of each trace. In the case where no molecule bridges the gap, the breaking traces show a featureless exponential conductance decrease, indicative of single-barrier tunneling. If a molecule contacts both electrodes, the conductance no longer follows this behavior. Instead, a slower conductance decay with plateau-like features is observed.

We present our data in the form of two-dimensional conductance versus displacement histograms built from 2000 consecutive traces. To check the presence of spurious contaminants in the MCBJ devices, 1000 traces are first recorded on the bare Au devices before they are exposed to the solvent with the molecules. Only if a clean junction was formed as indicated by clear single-barrier tunneling traces (see SI Figure S3), the molecules were deposited by pipetting a 2 μL drop of solution onto the sample. Subsequently, the solvent (dichloromethane) was allowed to evaporate. The molecules in this study consist of an n-phenylene backbone (n = 2, 3, 4) with alkynyl moieties at both sides (see Figure 1a). On each junction, calibration of the electrode displacement is done using the length of single-gold atom chains obtained from the 1000 traces on bare junctions before molecular deposition.[38,39]

Theoretical Calculations. The electronic ground-state properties were calculated using density functional theory (DFT) as implemented in the ADF package,[40,41] using the GGA-PBE functional,[42] and the triple-ζ plus polarization (TZP) Slater-type basis set. All electrons were considered, expect for the gold atoms were the frozen core approximation was used. The zeroth order regular approximation (ZORA) to the Dirac equation was used to account for relativistic effects due to the presence of the Au electrodes. Each molecule was connected to two pyramidal gold electrodes consisting of 30 atoms each. The geometries were converged to energy changes of less than 10^{-3} hartree, energy gradients of less than 10^{-3} hartree/Å maximum, and 6.7×10^{-4} hartree/Å RMS. We calculated the transmission through the molecular junction using the nonequilibrium Green's function (NEGF) formalism by connecting the outer gold layer to wide-band limit electrodes,[43] with a coupling strength of 1 eV. To correct for electron correlation errors upon addition/removal of a charge on the molecule, the DFT + Σ method was used,[8] implemented as follows. First, a correction to the ionization potential and electron affinity is calculated based on the anion and cation charge states of the molecule in gas phase. As gas phase geometry, the geometry of the molecule in the junction was chosen with the apex gold atoms attached. Second, image-charge effects were calculated for the different charge states (also in gas phase). This was done using the Hirschfeld charge distribution between two parallel plates, similar to a classic image charge model.[44,45] The image planes were set at a distance of 1 Å outside the innermost gold atoms.[8,46] Both contribution were combined to a scissor operator value for occupied and unoccupied levels and used to correct the transmission.

ASSOCIATED CONTENT

Supporting Information

The Supporting Information is available free of charge on the ACS Publications website at DOI: 10.1021/jacs.6b03383.

Synthesis details and conductance measurements and calculations (PDF)

AUTHOR INFORMATION

Corresponding Author

*H.S.J.vanderZant@tudelft.nl

Notes

The authors declare no competing financial interest.

ACKNOWLEDGMENTS

We acknowledge support from the Dutch organization for Fundamental Research (FOM), OCW/NWO, an ERC advanced grant (Mols@Mols), and the China scholarship council (CSC). We also acknowledge the Karlsruhe Nano Micro Facility (KNMF, www.kit.edu/knmf) of the Forschungszentrum Karlsruhe for provision of access to instruments at their laboratories.

REFERENCES

(1) Moth-Poulsen, K.; Bjørnholm, T. *Nat. Nanotechnol.* **2009**, *4*, 551−556.
(2) Nitzan, A.; Ratner, M. A. *Science* **2003**, *300*, 1384−1389.
(3) Aradhya, S. V.; Venkataraman, L. *Nat. Nanotechnol.* **2013**, *8*, 399−410.
(4) Schwarz, F.; Lörtscher, E. *J. Phys.: Condens. Matter* **2014**, *26*, 474201.

DOI: 10.1021/jacs.6b03383
J. Am. Chem. Soc. 2016, 138, 8465−8469

(5) Huang, Z.; Chen, F.; Bennett, P. A.; Tao, N. *J. Am. Chem. Soc.* **2007**, *129*, 13225−13231.
(6) Kiguchi, M.; Miura, S.; Hara, K.; Sawamura, M.; Murakoshi, K. *Appl. Phys. Lett.* **2006**, *89*, 213104.
(7) Kamenetska, M.; Quek, S. Y.; Whalley, A. C.; Steigerwald, M. L.; Choi, H. J.; Louie, S. G.; Nuckolls, C.; Hybertsen, M. S.; Neaton, J. B.; Venkataraman, L. *J. Am. Chem. Soc.* **2010**, *132*, 6817−6821.
(8) Quek, S. Y.; Venkataraman, L.; Choi, H. J.; Louie, S. G.; Hybertsen, M. S.; Neaton, J. B. *Nano Lett.* **2007**, *7*, 3477−3482.
(9) Li, Z.; Kosov, D. S. *Phys. Rev. B: Condens. Matter Mater. Phys.* **2007**, *76*, 035415.
(10) Hybertsen, M. S.; Venkataraman, L.; Klare, J. E.; Whalley, A. C.; Steigerwald, M. L.; Nuckolls, C. *J. Phys.: Condens. Matter* **2008**, *20*, 374115.
(11) Chen, F.; Li, X.; Hihath, J.; Huang, Z.; Tao, N. *J. Am. Chem. Soc.* **2006**, *128*, 15874−15881.
(12) Kristensen, I. S.; Mowbray, D. J.; Thygesen, K. S.; Jacobsen, K. W. *J. Phys.: Condens. Matter* **2008**, *20*, 374101.
(13) Zotti, L. A.; Kirchner, T.; Cuevas, J. C.; Pauly, F.; Huhn, T.; Scheer, E.; Erbe, A. *Small* **2010**, *6*, 1529−1535.
(14) Frisenda, R.; Tarkuç, S.; Galán, E.; Perrin, M. L.; Eelkema, R.; Grozema, F. C.; van der Zant, H. S. J. *Beilstein J. Nanotechnol.* **2015**, *6*, 1558−1567.
(15) Millar, D.; Venkataraman, L.; Doerrer, L. H. *J. Phys. Chem. C* **2007**, *111*, 17635−17639.
(16) Cheng, Z.-L.; Skouta, R.; Vázquez, H.; Widawsky, J. R.; Schneebeli, S.; Chen, W.; Hybertsen, M. S.; Breslow, R.; Venkataraman, L. *Nat. Nanotechnol.* **2011**, *6*, 353−357.
(17) Chen, W.; Widawsky, J. R.; Vazquez, H.; Schneebeli, S. T.; Hybertsen, M. S.; Breslow, R.; Venkataraman, L. *J. Am. Chem. Soc.* **2011**, *133*, 17160−17163.
(18) Hong, W.; Li, H.; Liu, S. X.; Fu, Y.; Li, J.; Kaliginedi, V.; Decurtins, S.; Wandlowski, T. *J. Am. Chem. Soc.* **2012**, *134*, 19425−19431.
(19) Widawsky, J. R.; Chen, W.; Vázquez, H.; Kim, T.; Breslow, R.; Hybertsen, M. S.; Venkataraman, L. *Nano Lett.* **2013**, *13*, 2889−2894.
(20) Hines, T.; Díez-Pérez, I.; Nakamura, H.; Shimazaki, T.; Asai, Y.; Tao, N. *J. Am. Chem. Soc.* **2013**, *135*, 3319−3322.
(21) Pla-Vilanova, P.; Aragonès, A. C.; Ciampi, S.; Sanz, F.; Darwish, N.; Diez-Perez, I. *Nanotechnology* **2015**, *26*, 381001.
(22) Ricci, A. M.; Calvo, E. J.; Martin, S.; Nichols, R. J. *J. Am. Chem. Soc.* **2010**, *132*, 2494−2495.
(23) Maity, P.; Takano, S.; Yamazoe, S.; Wakabayashi, T.; Tsukuda, T. *J. Am. Chem. Soc.* **2013**, *135*, 9450−9457.
(24) Zhang, Y.-Q.; Björk, J.; Weber, P.; Hellwig, R.; Diller, K.; Papageorgiou, A. C.; Oh, S. C.; Fischer, S.; Allegretti, F.; Klyatskaya, S.; Ruben, M.; Barth, J. V.; Klappenberger, F. *J. Phys. Chem. C* **2015**, *119*, 9669−9679.
(25) Kepčija, N.; Zhang, Y. Q.; Kleinschrodt, M.; Björk, J.; Klyatskaya, S.; Klappenberger, F.; Ruben, M.; Barth, J. V. *J. Phys. Chem. C* **2013**, *117*, 3987−3995.
(26) Martín, S.; Grace, I.; Bryce, M. R.; Wang, C.; Jitchati, R.; Batsanov, A. S.; Higgins, S. J.; Lambert, C. J.; Nichols, R. J. *J. Am. Chem. Soc.* **2010**, *132*, 9157−9164.
(27) Wold, D. J.; Haag, R.; Rampi, M. A.; Frisbie, C. D. *J. Phys. Chem. B* **2002**, *106*, 2813−2816.
(28) Querebillo, C. J.; Terfort, A.; Allara, D. L.; Zharnikov, M. *J. Phys. Chem. C* **2013**, *117*, 25556−25561.
(29) Adams, D. M.; Brus, L.; Chidsey, C. E. D.; Creager, S.; Creutz, C.; Kagan, C. R.; Kamat, P. V.; Lieberman, M.; Lindsay, S.; Marcus, R. A.; Metzger, R. M.; Michel-Beyerle, M. E.; Miller, J. R.; Newton, M. D.; Rolison, D. R.; Sankey, O.; Schanze, K. S.; Yardley, J.; Zhu, X. *J. Phys. Chem. B* **2003**, *107*, 6668−6697.
(30) Capozzi, B.; Dell, E. J.; Berkelbach, T. C.; Reichman, D. R.; Venkataraman, L.; Campos, L. M. *J. Am. Chem. Soc.* **2014**, *136*, 10486−10492.
(31) Xu, B. Q.; Li, X. L.; Xiao, X. Y.; Sakaguchi, H.; Tao, N. J. *Nano Lett.* **2005**, *5*, 1491−1495.
(32) Ford, M. J.; Hoft, R. C.; McDonagh, A. *J. Phys. Chem. B* **2005**, *109*, 20387−20392.
(33) Gao, H.-Y.; Franke, J.-H.; Wagner, H.; Zhong, D.; Held, P.-A.; Studer, A.; Fuchs, H. *J. Phys. Chem. C* **2013**, *117*, 18595−18602.
(34) McDonagh, A. M.; Zareie, H. M.; Ford, M. J.; Barton, C. S.; Ginic-Markovic, M.; Matisons, J. G. *J. Am. Chem. Soc.* **2007**, *129*, 3533−3538.
(35) Bowers, C. M.; Rappoport, D.; Baghbanzadeh, M.; Simeone, F. C.; Liao, K.-C.; Semenov, S. N.; Żaba, T.; Cyganik, P.; Aspuru-Guzik, A.; Whitesides, G. M. *J. Phys. Chem. C* **2016**, *120*, 11331−11337.
(36) Takahashi, S.; Kuroyama, Y.; Sonogashira, K.; Hagihara, N. *Synthesis* **1980**, *1980*, 627−630.
(37) Koshevoy, I. O.; Lin, C.-L.; Karttunen, A. J.; Jänis, J.; Haukka, M.; Tunik, S. P.; Chou, P.-T.; Pakkanen, T. A. *Inorg. Chem.* **2011**, *50*, 2395−2403.
(38) Martin, C. A.; van Ruitenbeek, J. M.; van der Zant, H. S. J. *Nanotechnology* **2010**, *21*, 265201.
(39) Martin, C. A.; Smit, R. H. M.; Egmond, R. V.; van der Zant, H. S. J.; van Ruitenbeek, J. M. *Rev. Sci. Instrum.* **2011**, *82*, 053907.
(40) te Velde, G.; Bickelhaupt, F. M.; Baerends, E. J.; Fonseca Guerra, C.; van Gisbergen, S. J. A.; Snijders, J. G.; Ziegler, T. *J. Comput. Chem.* **2001**, *22*, 931−967.
(41) Fonseca Guerra, C.; Snijders, J. G.; Te Velde, G.; Baerends, E. J. *Theor. Chem. Acc.* **1998**, *99*, 391−403.
(42) Perdew, J. P.; Burke, K.; Ernzerhof, M. *Phys. Rev. Lett.* **1996**, *77*, 3865−3868.
(43) Verzijl, C. J. O.; Seldenthuis, J. S.; Thijssen, J. M. *J. Chem. Phys.* **2013**, *138*, 094102.
(44) Neaton, J. B.; Hybertsen, M. S.; Louie, S. G. *Phys. Rev. Lett.* **2006**, *97*, 216405.
(45) Verzijl, C. J. O.; Celis Gil, J. A.; Perrin, M. L.; Dulić, D.; van der Zant, H. S. J.; Thijssen, J. M. *J. Chem. Phys.* **2015**, *143*, 174106.
(46) Perrin, M. L.; Verzijl, C. J. O.; Martin, C. A.; Shaikh, A. J.; Eelkema, R.; van Esch, J. H.; van Ruitenbeek, J. M.; Thijssen, J. M.; van der Zant, H. S. J.; Dulić, D. *Nat. Nanotechnol.* **2013**, *8*, 282−287.

DOI: 10.1021/jacs.6b03383
J. Am. Chem. Soc. 2016, 138, 8465−8469